International Journal of Smart and Nano Materials

ISSN: (Print) (Online) Journal homepage: https://www.tandfonline.com/loi/tsnm20

Optimal distribution of active piezoelectric elements for noise attenuation in sandwich panels

J. F. A. Madeira & A. L. Araujo

To cite this article: J. F. A. Madeira & A. L. Araujo (2020): Optimal distribution of active piezoelectric elements for noise attenuation in sandwich panels, International Journal of Smart and Nano Materials, DOI: 10.1080/19475411.2020.1829159

To link to this article: https://doi.org/10.1080/19475411.2020.1829159

Published online: 12 Oct 2020.

INTERNATIONAL JOURNAL OF SMART AND NANO MATERIALS
https://doi.org/10.1080/19475411.2020.1829159

Taylor & Francis
Taylor & Francis Group

Optimal distribution of active piezoelectric elements for noise attenuation in sandwich panels

J. F. A. Madeira[a,b] and A. L. Araujo[a]

[a]IDMEC, Instituto Superior Tecnico, Universidade de Lisboa, Lisboa, Portugal; [b]ADM, ISEL, Instituto Politecnico de Lisboa, Lisboa, Portugal

ABSTRACT

In this paper, a multiobjective optimization approach for obtaining the optimal distribution of surface-bonded piezoelectric sensors and actuators for noise attenuation in sandwich panels is presented. The noise attenuation is achieved by using negative velocity feedback control with co-located sensors and actuators. The control gains are also optimized in order to obtain the most efficient noise attenuation in a given frequency band. An in-house implementation of a viscoelastic soft core sandwich plate finite element, including surface-bonded piezoelectric sensors and actuators with active control capabilities, is used for obtaining the frequency response of the panels. The sound transmission capability of the panels is evaluated using the radiated sound power, along with the Rayleigh integral approach, which is suitable for lightly coupled structural/acoustic problems. The Direct MultiSearch (DMS) optimization algorithm is used to minimize the added weight due to the piezoelectric material, minimizing also the number of required controllers and maximizing the noise attenuation. The total length of the radiated sound power curve is shown to be an effective measure of noise attenuation in a given frequency band. Trade-off Pareto fronts and the obtained optimal configurations are presented and discussed.

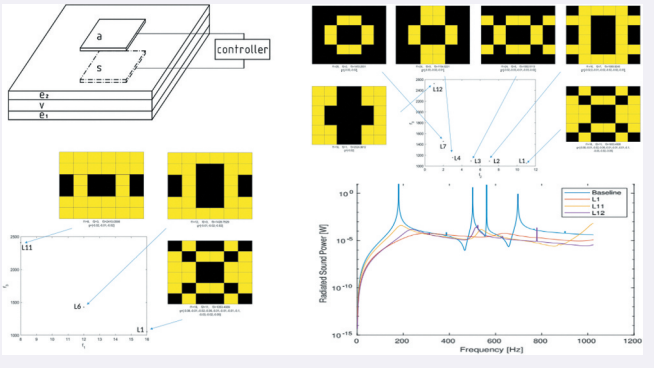

ARTICLE HISTORY
Received 4 June 2020
Accepted 20 August 2020

KEYWORDS
Sandwich structures; piezoelectricity; viscoelasticity; active damping; multiobjective optimization

CONTACT A. L. Araujo aurelio.araujo@tecnico.ulisboa.pt IDMEC, Instituto Superior Tecnico, Universidade de Lisboa, Portugal

1 Introduction

The structures used in the transportation industry are required to be lightweight for fuel efficiency reasons and, consequently, are prone to develop problems associated to high levels of vibration and noise transmission. The optimization of such structures for weight, cost, and vibration/noise attenuation is hence a fundamental issue in the modern transportation industry. Viscoelastic damping treatments are frequently used for damping vibrations, being most effective at higher frequencies, while piezoelectric sensors and actuators can give an important contribution at the lower end of the frequency spectrum. The combination of these two damping elements in a structure can thus improve the efficiency of vibration control and noise attenuation in a broader frequency band.

Some previous works regarding vibration and noise control using passive technologies have been presented in the last years, for mechanical vibration suppression [1] and sound level attenuation [2,3,4,5]. More recently, the vibroacoustic problem has been addressed by Larbi et al. in smart piezoelectric composite and sandwich plates [6,7,8,9,10] and also in double-wall sandwich panels [11,12]. The open literature regarding this subject of noise and vibration attenuation using both passive and active technologies is still quite scarce [13–16].

The present work is a generalization of the recent work on the optimal distribution of piezoelectric sensors and actuators in sandwich plate structures [13]. The purpose of the present approach is to show the importance of optimizing the control gains on the noise attenuation for these structures. Recently, noise attenuation in these sandwich panels has also been addressed by using shunted RL circuits [14,15], showing that this can be an alternative approach, especially if the cost of the controllers plays a major role, as the RL circuits are certainly less expensive than dedicated controllers. However, the active control strategy can achieve much more attenuated responses, depending only on the applied control gains.

A layerwise sandwich finite element model [17] is used in this work. In this model, the core of the sandwich is made of viscoelastic material with frequency-dependent properties, the face layers of the sandwich are made of laminated composite plies and piezoelectric patches are bonded to the outer surfaces of the skin layers and feedback control laws are used to increase damping. The model generates the frequency response of the panel when subjected to an external load and this response is then used to compute the radiated sound power of the sandwich plate in an unbounded surrounding acoustic medium. Multiobjective optimization is used to simultaneously minimize the weight of the added piezoelectric material and the added number of controllers required, while also minimizing noise emissions. The design variables are the distribution of the piezoelectric material on the plate surfaces and the control gains associated with the co-located control surfaces. The DMS (Direct MultiSearch) solver [18] is used, which is based on a novel technique called direct multisearch, developed by extending direct search from single to multiobjective optimization, using no information on derivatives of the objectives or constraints. It has been successfully used by the authors to solve problems of minimizing weight and maximizing damping of a viscoelastic sandwich plate [19], simultaneously minimizing weight and material cost and maximizing modal damping [20] and to find the optimal positioning of surface-bonded piezoelectric sensors and actuators for active damping maximization in a given frequency range [21]. An application is presented to

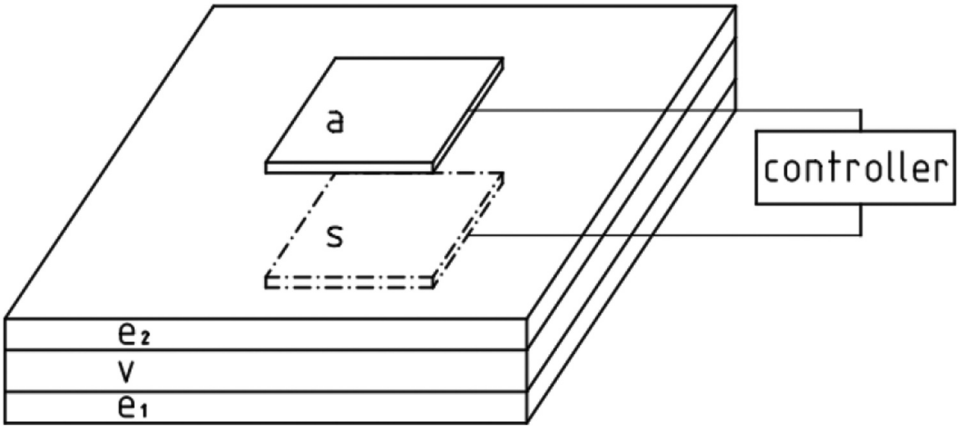

Figure 1. The active laminated plate model.

illustrate the importance of optimizing simultaneously the distribution of the piezoelectric patches and the control gains for effective attenuation of noise emissions.

2 Sandwich plate model

The developed in-house *layerwise* active sandwich finite element model represented in Figure 1 is briefly described in this section. The model addresses sandwich laminated plates with a viscoelastic (v) core, composite laminated face layers (e_1, e_2) and piezoelectric sensor (s) and actuator (a) layers bonded to the outer surfaces of the plate.

The following assumptions were made in the development of the sandwich plate model: The origin of the z axis is the mid-plane of the core layer; Perfect bonding is assumed at the interfaces between layers; The displacement is C^0 along the interfaces; Elastic and piezoelectric layers are modeled with first-order shear deformation theory (FSDT) and the viscoelastic core with a higher-order shear deformation theory (HSDT), using Taylor series expansions in the thickness coordinates which are cubic for the in-plane displacements and quadratic for the transverse displacement [17], allowing for transverse compressibility of the core; All materials are linear, homogeneous and orthotropic, and the elastic layers (e_1) and (e_2) are made of laminated composite materials; For the viscoelastic core (v), material properties are complex and frequency dependent; Bottom and top piezoelectric layers play the roles of sensor (s) and actuator (a), respectively, and are connected via feedback control laws, considering co-located control.

The FSDT displacement field of the face layers is written in the following form:

$$\begin{aligned} u^i(x,y,z,t) &= u_0^i(x,y,t) + (z-z_i)\theta_x^i(x,y,t) \\ v^i(x,y,z,t) &= v_0^i(x,y,t) + (z-z_i)\theta_y^i(x,y,t) \\ w^i(x,y,z,t) &= w_0^i(x,y,t) \end{aligned} \tag{1}$$

where u_0^i and v_0^i are the in-plane displacements of the mid-plane of the layer, θ_x^i and θ_y^i are rotations of normals to the mid-plane about the y axis (anticlockwise) and x axis (clockwise), respectively, w_0^i is the transverse displacement of the layer, z_i is the z coordinate of

the mid-plane of each layer, with reference to the core layer mid-plane ($z = 0$), and $i = s, e_1, e_2, a$ is the layer index.

For the viscoelastic core layer (v), the HSDT displacement field is written as a series expansion of the displacements in the thickness coordinate:

$$\begin{aligned} u^v(x,y,z,t) &= u_0^v(x,y,t) + z\theta_x^v(x,y,t) + z^2 u_0^{*v}(x,y,t) + z^3\theta_x^{*v}(x,y,t) \\ v^v(x,y,z,t) &= v_0^v(x,y,t) + z\theta_y^v(x,y,t) + z^2 v_0^{*v}(x,y,t) + z^3\theta_y^{*v}(x,y,t) \\ w^v(x,y,z,t) &= w_0^v(x,y,t) + z\theta_z^v(x,y,t) + z^2 w_0^{*v}(x,y,t) \end{aligned} \tag{2}$$

where u_0^v and v_0^v are the in-plane displacements of the mid-plane of the core, θ_x^v and θ_y^v are rotations of normals to the mid-plane of the core about the y axis (anticlockwise) and x axis (clockwise), respectively, w_0^v is the transverse displacement of the core mid-plane. The functions u_0^*v, v_0^*v, w_0^*v, θ_x^*v, θ_y^*v and θ_z^v are higher-order terms in the series expansion, defined also in the mid-plane of the core layer.

The model retains 19 mechanical unknowns, after enforcing displacement continuity at the layer interfaces. For more details on the model and its validation, the reader is directed to [17].

2.1 Constitutive relations

The materials for the composite laminated plies in the elastic face layers (e_1) and (e_2), viscoelastic core (v), and piezoelectric sensor (s) and actuator (a) layers are assumed orthotropic. For the laminas in the elastic laminated face layers and in the piezoelectric layers, constitutive equations for each lamina are expressed in the principal material directions, assuming zero transverse normal stress as in [22]. For the viscoelastic core, due to its transverse compressibility, a full 3D orthotropic stiffness matrix is used in the principal material directions [23] and the stiffness coefficients are complex quantities, since the complex modulus approach is used to obtain the frequency response, using the elastic-viscoelastic correspondence principle [24].

2.2 Finite element formulation

The extended Hamilton's principle is used for obtaining the equations of motion for the plate. The finite element method was employed to solve the equations of motion, using an eight-node serendipity element with 19 mechanical degrees of freedom per node, and one electric potential degree of freedom per piezoelectric layer. The system equilibrium equations, obtained through assembly of the element equations, are:

$$\begin{bmatrix} \mathbf{M}_{uu} & \mathbf{0} \\ \mathbf{0} & \mathbf{0} \end{bmatrix} \begin{bmatrix} \ddot{\mathbf{u}} \\ \ddot{\phi} \end{bmatrix} + \begin{bmatrix} \mathbf{K}_{uu} & \mathbf{K}_{u\phi} \\ \mathbf{K}_{u\phi}^T & \mathbf{K}_{\phi\phi} \end{bmatrix} \begin{bmatrix} \mathbf{u} \\ \phi \end{bmatrix} = \begin{bmatrix} \mathbf{F}_u \\ \mathbf{0} \end{bmatrix} \tag{3}$$

where $\mathbf{u}$, $\ddot{\mathbf{u}}$, ϕ and $\ddot{\phi}$ are mechanical degrees of freedom and corresponding accelerations, electric potential, and corresponding second time derivatives, respectively. $\mathbf{M}_{uu}$ and $\mathbf{K}_{uu}$ are the mass and complex stiffness matrices, respectively, corresponding to purely mechanical behavior, while $\mathbf{K}_{\phi\phi}$ is the dielectric stiffness matrix, $\mathbf{K}_{u\phi}$ is the stiffness matrix that corresponds to the coupling between the mechanical and the piezoelectric effects, and $\mathbf{F}_u$ is the externally applied mechanical load vector.

The assumed control laws (direct proportional or velocity feedback) can be written in the following form:

$$\phi_a = G_d\phi_s + G_v\dot{\phi}_s \tag{4}$$

where G_d and G_v are the constant displacement feedback gain and the constant velocity feedback gain, respectively, ϕ_a and ϕ_s are the vectors of actuator and sensor potentials, respectively, and $\dot{\phi}_s$ is the vector of sensor potential time derivatives.

The potential in the sensors can then be written as:

$$\phi_s = -\mathbf{K}_{\phi\phi_s}^{-1}\mathbf{K}_{u\phi s}^{T}\mathbf{u} \tag{5}$$

After assuming harmonic vibrations, the potentials in the actuators are written as:

$$\phi_a = -(G_d + i\omega G_v)\mathbf{K}_{\phi\phi_s}^{-1}\mathbf{K}_{u\phi s}^{T}\mathbf{u} \tag{6}$$

Finally, the equilibrium equations are given by:

$$\left[\mathbf{K}^{*}(\omega) - \omega^2\mathbf{M}_{uu}\right]\mathbf{u} = \mathbf{F}_u \tag{7}$$

where the non-symmetric condensed stiffness matrix is given by:

$$\mathbf{K}^{*}(\omega) = \mathbf{K}_{uu}(\omega) - \left[(G_d + i\omega G_v)\mathbf{K}_{u\phi_a} + \mathbf{K}_{u\phi_s}\right]\mathbf{K}_{\phi\phi_s}^{-1}\mathbf{K}_{u\phi s}^{T} \tag{8}$$

and $\mathbf{K}_{uu}(\omega)$ is a complex matrix.

When electroded surfaces are present in a certain patch or layer, equipotential conditions are imposed on the electrodes before condensing the electric degrees of freedom. This is accomplished by choosing one master potential degree of freedom on the patch and imposing all the others on that particular patch equal to the master.

The forced vibration problem is solved in the frequency domain, which translates in the solution of the following linear system of equations for each frequency point:

$$\left[\mathbf{K}^{*}(\omega) - \omega^2\mathbf{M}_{uu}\right]\mathbf{u}(\omega) = \mathbf{F}_u(\omega) \tag{9}$$

where $\mathbf{F}_u(\omega) = \mathcal{F}(\mathbf{F}_u(t))$ is the Fourier transform of the time domain force history $\mathbf{F}_u(t)$.

3 Radiated sound power

A panel radiates noise into the surrounding acoustic medium when it is subject to external excitation. While for light fluids, the effect of the fluid mass may be neglected and the acoustic and structural problems can be solved independently, for a heavy fluid, due to strong acoustic radiation damping and added mass effects, the problem is not so simple as the inertia of the coupled structure is significantly influenced. In the present study we deal with radiation involving light fluids such as air, hence the fluid loading is neglected. The radiated sound power (Π) is the acoustic indicator chosen to evaluate the acoustic performance of the active sandwich panels.

The sound power radiated through a plate with surface area S is given by:

$$\Pi = \frac{1}{2}\Re\left(\int_S p(P)v_n^{H}(P)dS\right) \tag{10}$$

where P is a point on the plate surface, p is the sound pressure applied as an external loading and v_n is the normal velocity at the surface of the panel. The hermitian transpose is denoted by ^{H} and $\Re$ denotes the real part of the integral.

For a flat plate embedded in an infinite rigid plane baffle and radiating to a semi-infinite fluid, the pressure p is obtained using the Rayleigh Integral [25]:

$$p(\omega, M) = \rho_0 \frac{i\omega}{2\pi} \int_S v_n(\omega, P) \frac{e^{-ikr}}{r} dS \tag{11}$$

where ρ_0 is the mass density of the acoustic domain, $k = \omega/c_0$ is the wavenumber, c_0 is the speed of sound in air, M is a point inside the external acoustic domain and $v_n(\omega, P)$ is the normal velocity at point P, easily obtained from the finite element model presented above.

A sufficient number of discrete radiating elements, according to the smallest wavelength to be observed, is used in the finite element method to obtain the normal velocity distribution, where the normal velocities at the center positions of each rectangular finite element is considered. The dimensions of these elements are small when compared to the structural and acoustic wavelengths, so that the total radiated sound power in Equation (10) can be expressed as the sum of the powers radiated by each element:

$$\Pi = \frac{S_e}{2} \Re\left(\mathbf{v}_n^H \mathbf{p}\right) \tag{12}$$

where the superscript ^{H} denotes the hermitian transpose, $\mathbf{v}_n$ and $\mathbf{p}$ are the vectors of complex amplitudes of the normal velocity and acoustic pressure at the element center locations, respectively, and S_e is the surface area of each element. The pressure on each element is generated by the vibrations of all elements of the panel and the vector of sound pressures is then obtained using the impedance matrix:

$$\mathbf{p} = \mathbf{Z}\mathbf{v}_n \tag{13}$$

where $\mathbf{Z}$ is the (symmetric) impedance matrix with components:

$$Z_{ij} = \left(i\omega\rho_0 S_e / 2\pi r_{ij}\right) e^{-ikr_{ij}} \tag{14}$$

and r_{ij} is the distance between the centers of the elements i and j. Substituting Equation (13) in Equation (12), we obtain:

$$\Pi = \frac{S_e}{2} \Re\left(\mathbf{v}_n^H \mathbf{Z}\mathbf{v}_n\right) = \frac{S_e}{4} \Re\left(\mathbf{v}_n^H \left[\mathbf{Z} + \mathbf{Z}^H\right] \mathbf{v}_n\right) = \mathbf{v}_n^H \mathbf{R} \mathbf{v}_n \tag{15}$$

where $\mathbf{R}$ is the radiation resistance matrix for the elementary radiators which is given by:

$$\mathbf{R} = \frac{\omega^2 \rho_0 S_e^2}{4\pi c_0} \times \begin{bmatrix} 1 & \frac{\sin(kr_{12})}{kr_{12}} & \cdots & \frac{\sin(kr_{1R})}{kr_{1R}} \\ \frac{\sin(kr_{21})}{kr_{21}} & 1 & \cdots \frac{\sin(kr_{2R})}{kr_{2R}} & \\ \vdots & \vdots & \ddots & \vdots \\ \frac{\sin(kr_{R1})}{kr_{R1}} & \frac{\sin(kr_{R2})}{kr_{R2}} & \cdots & 1 \end{bmatrix} \tag{16}$$

This method is applicable to any plane surface in an infinite baffle, independently of the boundary conditions, as it only requires the knowledge of the surface geometry, the properties of the fluid, and the normal velocity field distribution.

4 Problem statement

A sandwich plate is considered in this application. The plate has a viscoelastic core and laminated face sheets. The behavior of the viscoelastic core material is described by a fractional derivative constitutive law. The plate has in-plane dimensions 300 mm $\times$ 200 mm and all edges are clamped. The face sheets are made of carbon fiber plies with stacking sequence $[0^\circ/90^\circ/+45^\circ]$ for (e_1) and $[+45^\circ/90^\circ/0^\circ]$ for (e_2). The thickness of each carbon fiber ply is 0.5 mm, and the viscoelastic core is 2.5 mm thick.

A five-parameter fractional derivative constitutive model [26] is used to describe the material properties of the isotropic viscoelastic damping polymer used for the core of the sandwich. For this material $v = 0.49$ and $\rho = 1300$ kg/m^3, have been assumed. The complex shear modulus can be expressed as follows:

$$G(j\omega) = G_0 + G_0(d-1)\frac{(j\omega\tau)^\alpha}{1+(j\omega\tau)^\beta} \tag{17}$$

where $G_0 = 0.8$ MPa is the static shear modulus, $d = 1$, $\alpha = 0.566$, $\beta = 0.558$, and $\tau = 7.23 \times 10^{-10}$ s is the relaxation time.

For the carbon fiber plies, the material properties are $E_1 = 130.8$ GPa, $E_2 = 10.6$ GPa, $G_{12} = 5.6$ GPa, $G_{13} = 4.2$ GPa, $G_{23} = 3.0$ GPa, $v_{12} = 0.36$, and $\rho = 1543$ kg/m^3.

Co-located pairs of piezoelectric surface electroded patches with 0.9 mm thickness can be bonded to the upper and lower surfaces of the plate. Material properties for these piezoelectric patches are $E_1 = 50.9$ GPa, $E_2 = 46.1$ GPa, $G_{12} = 14.3$ GPa, $G_{13} = 8.0$ GPa, $G_{23} = 20.6$ GPa, $v_{12} = 0.29$, $\rho = 7800$ kg/m^3, $e^*_{31} = -17.0$ N/Vm, $e^*_{32} = -12.2$ N/Vm, and $\in^{*\varepsilon}_{33} = 1.549 \times 10^{-8}$ F/m. The (*) in the piezoelectric and dielectric properties indicate that these are reduced plane stress properties [22].

A 100 Pa incident pressure wave is applied to the plate bottom surface at $t = 0$. For the control gains in Eq. (4), $G_d = 0$ is fixed and G_v is a design variable.

The optimization problem is formulated in such a way to find optimal distributions of the co-located pairs of piezoelectric patches on the surfaces of the sandwich panel, and at the same time optimize the velocity G_v control gains for the patches. Three objectives are defined: The first objective is to minimize the added mass of the patches $f_1 = \sum_i m_i$, where m_i is the mass of the double patches of element i; The second objective is to minimize the number of equipotential zones f_2 at in the patch distribution, corresponding to the minimization of the total number of individual controllers needed to impose the negative velocity feedback control gain to each equipotential zone; The third objective is the maximization of damping over a frequency band of interest, which in the current application corresponds to the interval from 0 Hz to 1024 Hz. This last objective is implemented using two distinct objective functions with the goal of comparing their relative performance: minimization of the total length f_3 of the radiated sound power curve defined through Eq. (15) in Section 3, and minimization of the maximum value of the same radiated sound power curve. Therefore, two distinct optimizations are

conducted in this study and their results in terms of the performance of the optimal solutions obtained are compared in the end. The optimization problem is stated as:

$$\begin{array}{ll} \min & F(x) \equiv (f_1(x), f_2(x), f_3(x))^{\mathrm{T}} \\ \text{s. t.} & \phi_j \leq 100\,\mathrm{V}, \qquad j = 1, \ldots 18 \\ & x_i \in \{0, 1\}, \qquad i = 1, \ldots, 9 \\ & x_i \in [-0.1, 0], \qquad i = 10, \ldots, 27 \end{array} \tag{18}$$

where $f_3(x)$ can be either the total length of the radiated sound power curve or the maximum amplitude value of the curve. The design variable x_i for $i = 1, \ldots, 9$ takes values of 0 or 1, where the zero value means that there is no patch and a one represents a pair of co-located patches at that particular element i. Since DMS uses real valued design variables and our problem has by nature discrete variables, for the optimization we consider a vector of real variables in the interval [0,1] with length equal to the number of elements in the mesh. If a certain design variable value is greater or equal to 0.5, we consider that the patch exists, i.e., it will be rounded to one, otherwise the patch is not present at that particular element, and the value of the variable is rounded to zero for function evaluation purposes.

In the present work, symmetry conditions on the distribution of the piezoelectric patches are considered. The finite element mesh is a 6×6 regular mesh with a total of 36 rectangular elements. Therefore, only nine design positioning variables are considered due to symmetry, corresponding to a quarter of the plate.

As for the design variables x_i for $i = 10, \ldots, 27$, they represent the negative feedback control gains in each equipotential zone. Each negative feedback gain is allowed to vary from -0.1 to 0 in increments of 0.01. The maximum number of control gains is 18, which coincides with the maximum number of equipotential zones in a checkerboard configuration for the 6×6 finite element mesh.

Constraints on the electric potentials ϕ_j on each one of the equipotential zones are also imposed in order to prevent applied voltages to the actuators higher than 100 V. In this way we minimize the risk of depolarizing the piezoelectric patches through to the application of very high electric fields.

It should be noted that the patches are not clamped and only the base plate is clamped along the edges. The coarse mesh used in this work is justified by the high number of function evaluations that are required by the optimization algorithm, as computational time must be kept at a reasonable level. If a more refined mesh is needed (the solutions are mesh dependent), the results from the current optimization are used as a starting point for the new optimization with the finer mesh. Examples of the mesh dependency on the optimization results using this formulation for passive damping treatments can be found in [27], where it can be seen that undesired checkerboard patterns become an issue when very refined meshes are used. Furthermore, for the frequency band considered in this work, with a maximum frequency of 1024 Hz, a 6×6 mesh is adequate from the point of view of minimum wavelength.

The Direct MultiSearch (DMS) [18] solver is used in this work. DMS does not use derivatives and does not aggregate any components of the objective function. It essentially generalizes all direct-search methods of directional type from single to multiobjective optimization. DMS maintains a list of feasible non-dominated points (from which the new iterates or poll centers are chosen). The search step is optional and when included it

aims at improving numerical performance. DMS tries, however, to capture the whole Pareto front from the polling procedure itself. At each iteration, the new feasible evaluated points are added to this list and the dominated ones are removed. Successful iterations correspond to changes in the iterate list, meaning that a new feasible nondominated point was found. Otherwise, the iteration is declared as unsuccessful.

When a point is infeasible, the components of the objective function F are not evaluated, and the values of F_Ω are set to $+\infty$. This approach allows to deal with black-box type constraints, where only a yes/no type of answer is returned. A number of details of the algorithm are omitted and the reader is referred to [18] for a complete description. The authors in [18] prove under the common assumptions used in direct search for single-objective optimization that at least one limit point of the sequence of iterates generated by DMS lies in (a stationary form of) the Pareto front.

5 Results

In this section, we present the results obtained for the multiobjective optimization, for the two distinct objective functions considered for f_3. In the first case f_3 will be the total length of the radiated sound power curve, taking into consideration that we wish to minimize the response over the considered frequency range, and the minimum length curve will tend to represent a configuration where the response has the lowest possible amplitude over this frequency range. In the second case, we consider the minimization of the maximum value of the radiated sound power curve in the same frequency range, which is a rather classical approach for this type of problems [28].

5.1 Minimization of the total length of the RSP curve

For this choice of the objective function f_3, there are a total of 15 nondominated solutions. As the fundamental objective is the maximization of damping (objective f_3), Figure 2 shows the nondominated solutions in the $f_1 - 3_1$ and $f_2 - f_3$ planes.

One can observe that solution L11 is the lightest one with $f_1 = 8$, $f_2 = 3$ and $f_3 = 2410.1$. However, this is not the solution with the lowest damping. Solution L12 ($f_1 = 16, f_2 = 1, f_3 = 2525.0$) corresponds to the highest value of the curve length (f_3) and hence is the least damped solution, with just one controller. On the other hand, solution L1 has the largest amount of added piezoelectric patches ($f_1 = 16$) and the highest damping – lowest curve length ($f_3 = 1053.5$). Solution L1 is also the solution associated to the highest number of controllers ($f_2 = 11$).

Figure 3 displays the radiated sound power for the three solutions L1, L11, and L12, for comparison purposes, along with the baseline solution, which corresponds to the base plate without any added piezoelectric patches. The effect of the noise reduction can be clearly noticed from these response curves. The optimal control gains are provided for solutions L1, L11, and L12 in Table 1.

5.2 Minimization of the maximum value of the RSP curve

In the case where the objective function f_3 corresponds to the maximum value of the radiated sound power curve, there are a total of 11 nondominated solutions and. Again, as

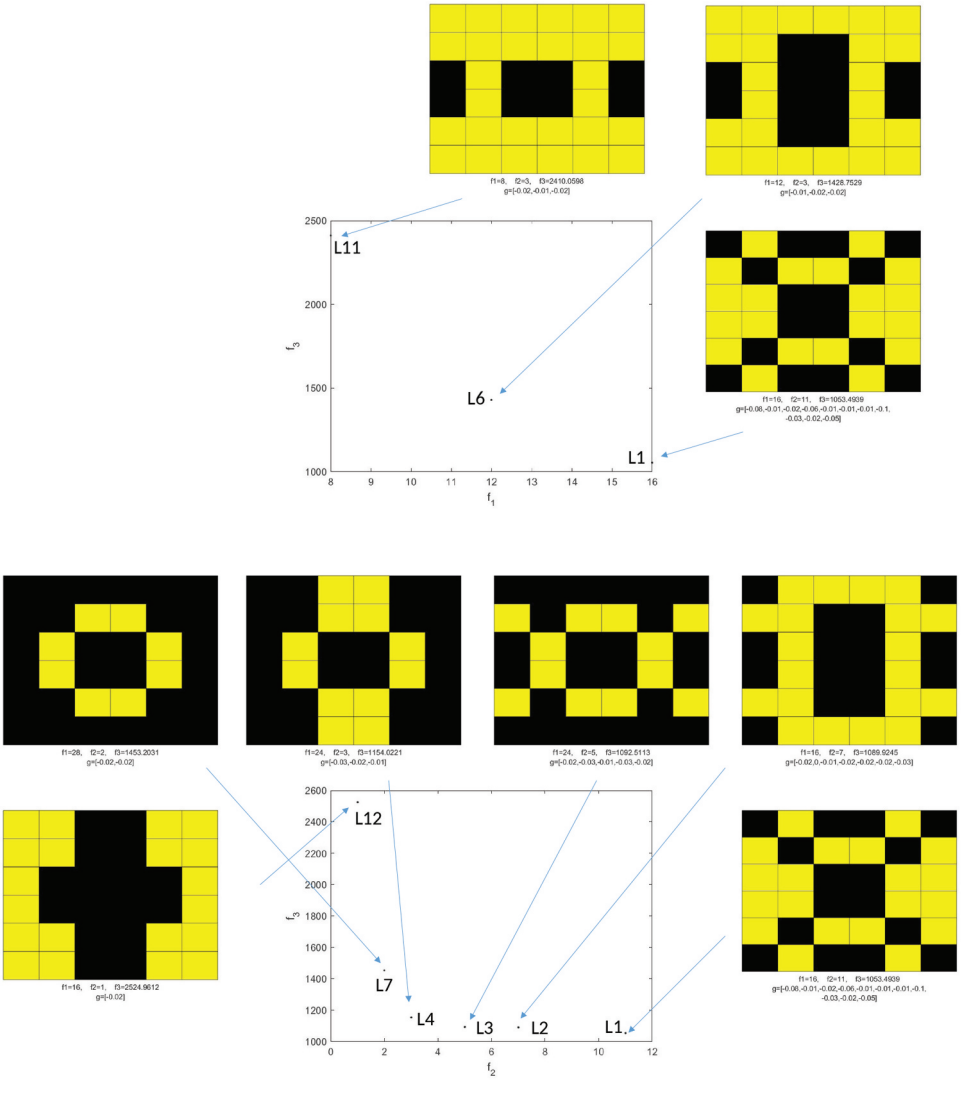

Figure 2. Minimization of the total length of the radiated sound power curve: nondominated solutions with respect to damping (curve length f_3) versus added mass (number of added piezoelectric pairs f_1) and number of equipotential zones (number of controllers f_2).

the fundamental objective is the maximization of damping (objective f_3), Figure 4 shows the nondominated solutions in the $f_1 - f_3$ and $f_2 - f_3$ planes. The optimal control gains are provided for selected solutions M10, M5, and M3 in Table 1.

Table 2 presents the first six natural frequencies and modal loss factors for the optimal solutions L1/M10, L11/M5, L12/M3, along with the baseline solution (sandwich plate with no added piezoelectric patches). It should be noted that the base plate is in fact undamped due to the choice of $d = 1$ in Equation 17. This was done to enhance the effect of the active damping introduced by the negative velocity feedback. In fact, it can be seen both in Table 2 and in Figure 3 that quite a substantial amount of damping is

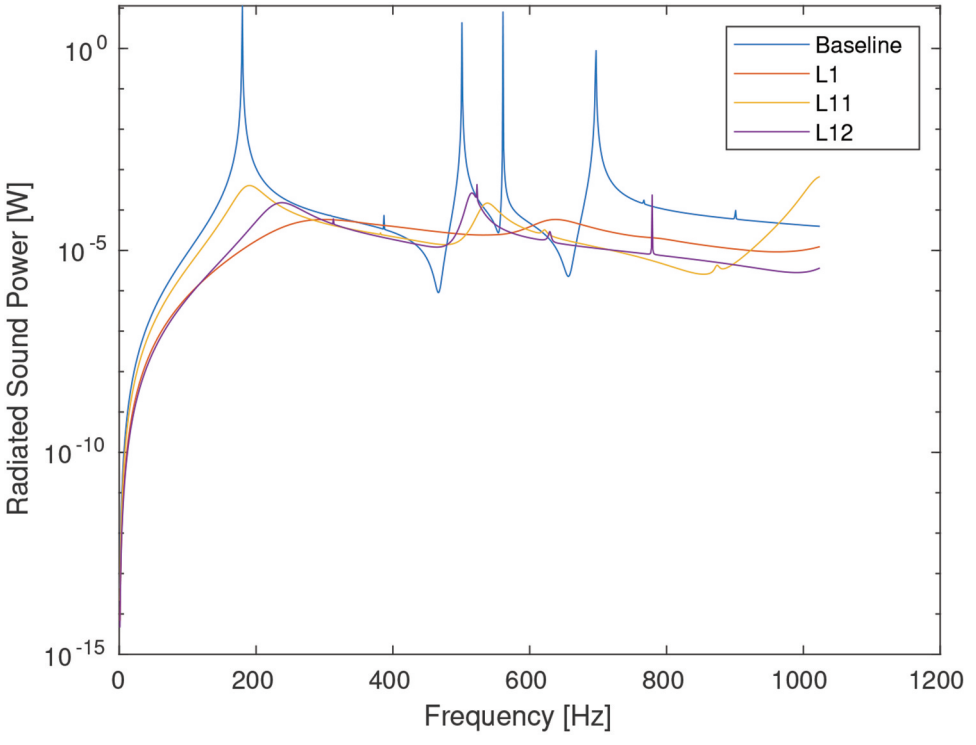

Figure 3. Minimization of the total length of the radiated sound power: radiated round power for solutions L1, L11, L12 and baseline solution (no added piezoelectric patches).

Table 1. Optimal control gains for highlighted optimal solutions. Solutions L1 and M10 and L12 and M3 are identical. Solutions L11 and M5 share the same patch distribution, but with different control gains. Gains are ordered from left to right and from bottom to top, with respect to the patch distribution.

Solution	Control gains G_v
L1/M10	−0.08, −0.01, −0.02, −0.06, −0.01, −0.01, −0.01, −0.1, −0.03, −0.02, −0.05
L11/M5	−0.02/-0.01, −0.01, −0.02/-0.0
L12/M3	−0.02

added by the feedback control law, especially in the first mode of vibration. This confirms the effectiveness of active damping in the low frequencies.

The natural frequencies and modal loss factors in Table 2 were obtained from the solution of the following non-linear eigenvalue problem:

$$\left[\mathbf{K}^*(\omega) - \lambda_n^* \mathbf{M}_{uu}\right]\mathbf{u}_n = \mathbf{0} \tag{19}$$

where the complex eigenvalue λ_n^* is written as:

$$\lambda_n^* = \lambda_n(1 + i\eta_n) \tag{20}$$

and $\lambda_n = \omega_n^2$ is the real part of the complex eigenvalue and η_n is the corresponding modal loss factor.

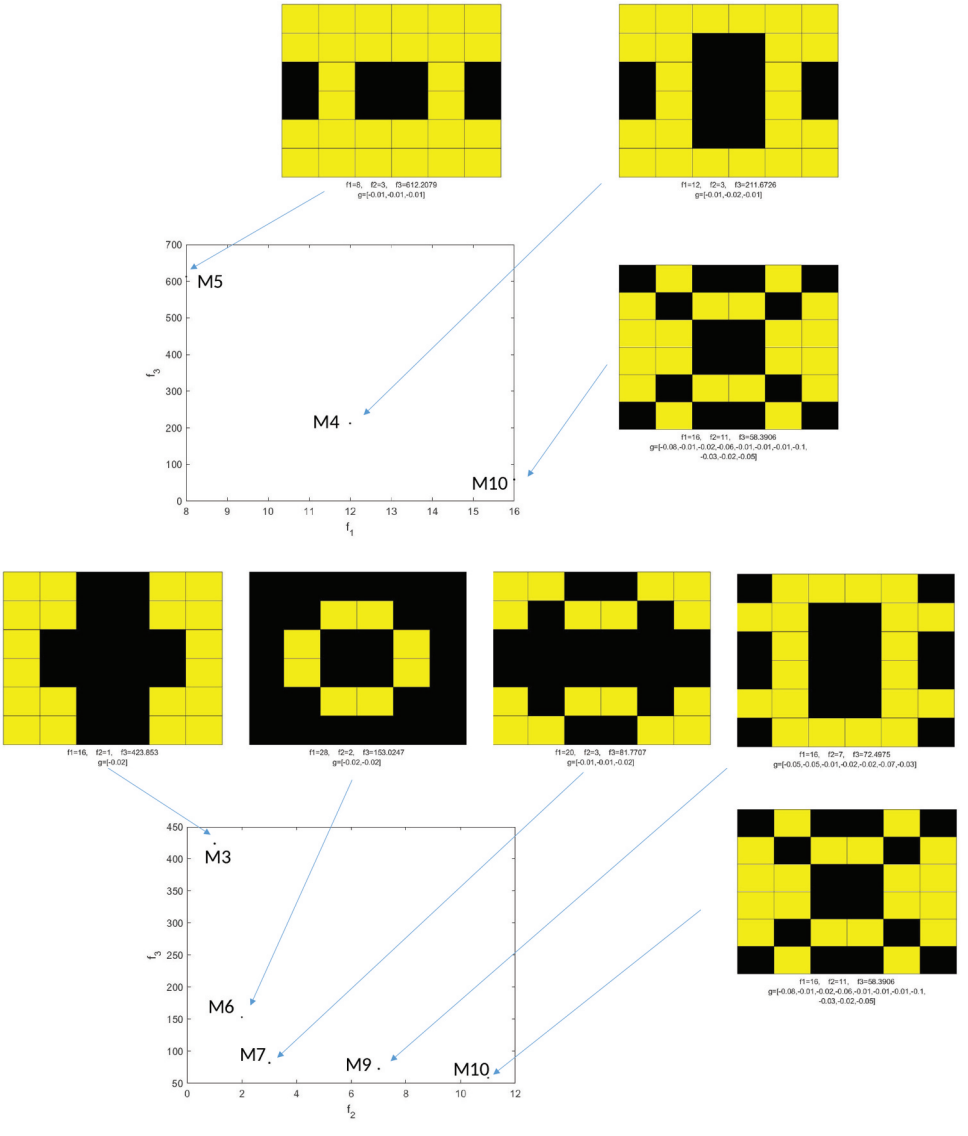

Figure 4. Minimization of the maximum value of the radiated sound power: nondominated solutions with respect to damping (maximum curve value f_3) versus added mass (number of added piezoelectric pairs f_1) and number of equipotential zones (number of controllers f_2).

The non-linear eigenvalue problem was solved iteratively and the iterative process is considered to have converged when:

$$\frac{\| \omega_i - \omega_{i-1} \|}{\omega_{i-1}} \leq \in \tag{21}$$

where ω_i and ω_{i-1} are current and previous iteration values for the real part of the particular eigenfrequency of interest, respectively, and $\in = 1 \times 10^{-6}$ is the convergence tolerance.

Table 2. First six natural frequencies f_i [Hz] and modal loss factors η_i [%] for the optimal solutions L1/M10, L11/M5, L12/M3, and the baseline solution (sandwich plate with no added piezoelectric patches).

	Baseline		L1/M10		L11/M5		L12/M3	
i	f_i	η_i	f_i	η_i	f_i	η_i	f_i	η_i
1	179.83	0.00	256.94	54.06	186.02	21.41	231.30	25.48
2	309.38	0.00	374.42	17.13	308.25	3.75	313.12	0.00
3	387.11	0.00	537.06	9.32	381.78	0.01	514.18	3.44
4	501.10	0.00	624.37	13.95	534.20	5.96	522.76	0.01
5	560.98	0.00	782.89	8.40	621.41	1.26	629.61	0.67
6	696.64	0.00	811.00	6.28	706.58	1.06	778.88	0.00

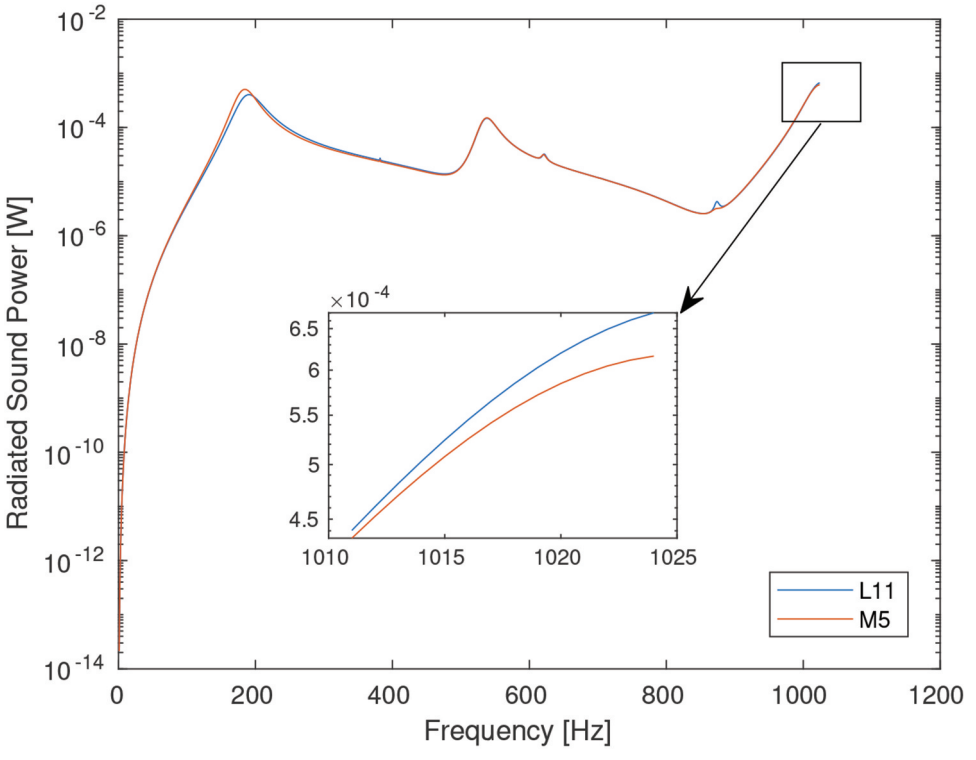

Figure 5. Comparison of the radiated sound powers of solutions M5 and L11.

6 Discussion

One can observe from the results that most of the solutions obtained using the minimization of either the total length or the maximum value of the radiated sound power curves are similar, with respect to the piezoelectric material distribution. Hence, solutions M10 and solutions L1 are identical and correspond to the best possible solution for maximizing damping in this frequency range. On the other hand, the solution M3 that uses the least number of controllers is no longer the least damped solution in this optimization. In fact, solution M5, which in terms of material distribution is identical to solution L11, is now the least damped solution and the lightest one. In fact, solutions M5 and L11 are identical in terms of the piezoelectric material configuration but they differ in

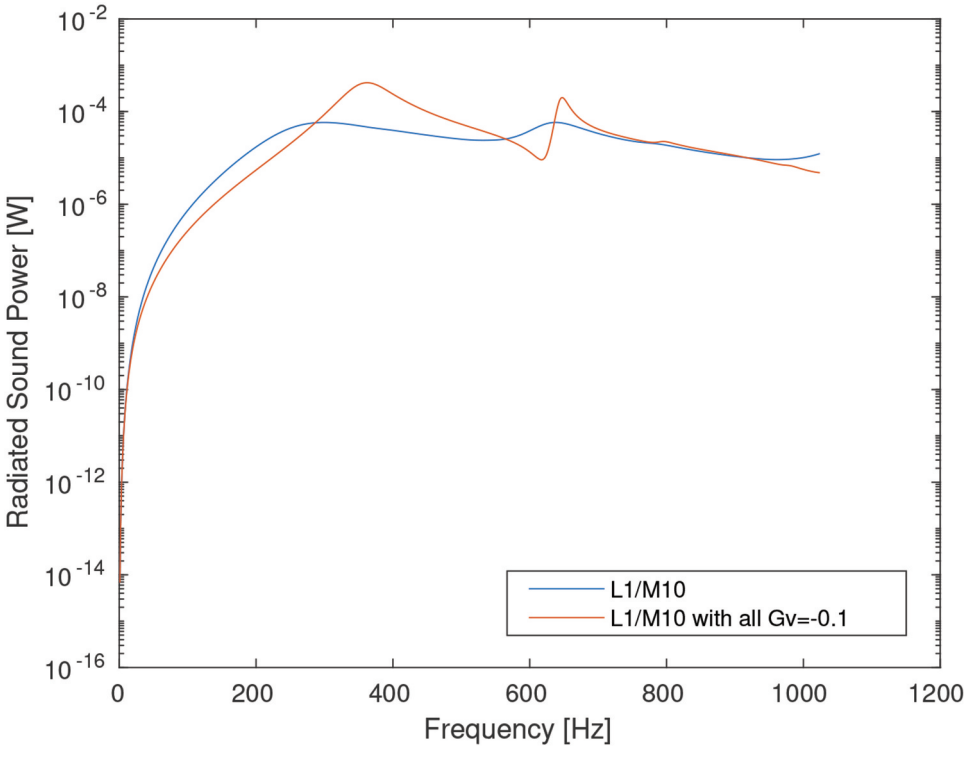

Figure 6. Comparison of the radiated sound powers of best solution for damping L1/M10 with optimal versus maximum control gains.

terms of control gains: while in solution M5 all gains are set to −0.01, in the case of L11, two of these gains are set to −0.02 (see Table 1). These two response curves can be observed in Figure 5, where it is evident that, although solution L11 seems overall better than solution M5 (which seems natural due to the higher control gains that are applied), the maximum value of these curves is really attained at frequency 1024 Hz (last point of the curve), where L11 presents a slightly higher response value than M5. Hence, the total length of the radiated sound power curve is not so sensitive to local fluctuations in a given frequency range as the absolute maximum value is. This suggests that the total length of the curve is a better estimate for the overall damping capability and noise attenuation in a given frequency band, when compared to the maximum value of the curve.

Regarding the optimal distribution of the control gains, since negative velocity feedback mainly contributes to the increase of active damping of a structure, one might think that larger values for these gains would always be preferable in terms of increasing the damping capability of a particular structures. In order to check this, a new radiated sound power curve was obtained for the most damped solution found in the Pareto fronts (L1/M10), where all control gains were set to the maximum possible absolute value $G_v = -0.1$. The results are displayed in Figure 6, where it can be clearly seen that the increase in the absolute values of the control gains produces a less damped solution when compared to the optimal solution. In fact, in this figure, the response levels are overall much higher when control gains are increased beyond the optimal values. This illustrates the importance of

obtaining not only the optimal distribution of piezoelectric patches but also the optimal values of the control gains that maximize noise attenuation in a given frequency band.

As for the values of the applied potentials in the actuators, since these have been constrained in the optimization formulation in Equation (18), their values are always kept below 100 V. In the particular case of solution L1/M10, the maximum applied voltage is around 83 V. However, when the control gains are all set to −0.1, this value increases up to 277 V, far beyond the upper limit that was defined in the formulation. Hence, we see that both noise attenuation and control voltages do limit the values of the applied gains in this problem.

7 Conclusions

Multiobjective optimization has been used in this work in order to obtain the best distribution of surface-bonded co-located piezoelectric patches in laminated sandwich panels with viscoelastic core, for reducing acoustic emissions, using negative velocity feedback control. The problem is formulated with three objectives: the reduction of acoustic emissions is accomplished through the damping introduced by the control elements, while minimizing the added mass of the piezoelectric material and the number of controllers that are required. Two different indicators are used for assessing the damping capability of the structure in a given frequency band: the total length of the radiated sound power curve and its maximum value. The optimization results are compared and the conclusions point out that the total length of the curve is a better indicator for overall damping in a given frequency range, due to the fact that it is not so sensitive to local perturbations in the curve. The importance of simultaneously addressing the distribution of the co-located piezoelectric sensors and actuators and the patch control gains is also illustrated by analyzing the obtained results. This methodology proved to be efficient in minimizing noise transmission over a given frequency range, while keeping the added mass and the number of controllers to a minimum. Future extensions of the current work will deal with the mesh dependency issue by improving the computational efficiency of the codes and simultaneously dealing with the checkerboard problems that naturally arise when using more refined meshes.

Data availability

The data that support the findings of this study are available from the corresponding author upon reasonable request.

Disclosure statement

No potential conflict of interest was reported by the authors.

Funding

This work has been supported by National Funds through Fundação para a Ciência e Tecnologia (FCT), through IDMEC, under LAETA, project [UIDB/50022/2020].

References

[1] Rao MD. Recent applications of viscoelastic damping for noise control in automobiles and commercial airplanes. J Sound Vib. 2003;262(3):457–474.

[2] Foin O, Nicolas J, Atalla N. An efficient tool for predicting the structural acoustic and vibration response of sandwich plates in light or heavy fluid. Appl Acoust. 1999;57(3):213–242.

[3] Subramanian S, Surampudi R, Thomson KR, et al. Optimization of damping treatments for structure borne noise reduction. J Sound Vib. 2004;38(9):14–18.

[4] Assaf S, Guerich M, Cuvelier P. Vibration and acoustic response of damped sandwich plates immersed in a light or heavy fluid. Comput Struct. 2010;88(13–14):870–878.

[5] Loredo A, Plessy A, El Hafidi A, et al. Numerical vibroacoustic analysis of plates with constrained layer damping patches. J Acoust Soc Am. 2011;129(4):1905–1918.

[6] Larbi W, Deü JF, Ohayon R. Finite element formulation of smart piezoelectric composite plates coupled with acoustic fluid. Compos Struct. 2012;94:501–509.

[7] Larbi W, Deü JF, Ohayon R. Finite element reduced order model for noise and vibration reduction of double sandwich panels using shunted piezoelectric patches. Appl Acoust. 2016;108:40–49.

[8] Larbi W. Numerical modeling of sound and vibration reduction using viscoelastic materials and shunted piezoelectric patches. Comput Struct. 2020;232:105822.

[9] Larbi W, da Silva LP, Deü J-F. An efficient fe approach for attenuation of acoustic radiation of thin structures by using passive shunted piezoelectric systems. Appl Acoust. 2017;128:3–13.

[10] Larbi W, Deü J-F, Pereira da Silva L. Design of shunted piezoelectric patches using topology optimization for noise and vibration attenuation. Appl Condit Monitor. 2017;5:23–33.

[11] Larbi W, Deü JF, Ohayon R. Vibroacoustic analysis of double-wall sandwich panels with viscoelastic core. Comput Struct. 2016;174:92–103.

[12] Soussi C, Larbi W, Deü J-F. Experimental and numerical analysis of sound transmission loss through double glazing windows. Appl Condit Monitor. 2019;13:195–203.

[13] Araújo AL, Madeira JFA. Multiobjective optimization solutions for noise reduction in composite sandwich panels using active control. Compos Struct. 2020;247:112440.

[14] Araújo AL, Aguilar Madeira JF. Optimal passive shunted damping configurations for noise reduction in sandwich panels. JVC/J Vibrat Cont. (in press), 2020;26:1110–1118.

[15] Vieira FS, Araujo AL. Implementation of a PID controller in ANSYS for noise reduction applications. Mech Adv MaterStruct. (in press), 2019,26(13–14):1110–1118.

[16] Vieira FS, Araújo AL. Optimization and modelling methodologies for electro-viscoelastic sandwich design for noise reduction. Compos Struct. 2020;235.111778.

[17] Araujo AL, Carvalho VS, Mota Soares CM, et al. Vibration analysis of laminated soft core sandwich plates with piezoelectric sensors and actuators. Compos Struct. 2016;151:91–98.

[18] Custódio AL, Madeira JFA, Vaz AIF, et al. Direct multisearch for multiobjective optimization. SIAM J Optimizat. 2011;21:1109–1140.

[19] Madeira JFA, Araújo AL, Mota Soares CM, et al. Multiobjective optimization of viscoelastic laminated sandwich structures using the direct multisearch method. Comput Struct. 2015;147:229–235.

[20] Madeira JFA, Araújo AL, Mota Soares CM, et al. Multiobjective design of viscoelastic laminated composite sandwich panels. Compos Part B. 2015;77:391–401.

[21] Araújo AL, Madeira JFA, Mota Soares CM, et al. Optimal design for active damping in sandwich structures using the direct multisearch method. Compos Struct. 2013;105:29–34.

[22] Araújo AL, Lopes HMR, Vaz MAP, et al. Parameter estimation in active plate structures. Comput Struct. 2006;84:1471–1479.

[23] Reddy JN. Mechanics of laminated composite plates and shells: theory and analysis. 2nd ed. Boca Raton: CRC Press; 2004.

[24] Christensen RM. Theory of Viscoelasticity. 2nd ed. New York: Academic Press; 1982.

[25] Fahy F, Gardonio P. Sound and structural vibration: radiation, transmission and response. 2nd ed. Academic Press; 2006. Oxford.

[26] Pritz T. Five-parameter fractional derivative model for polymeric damping materials. J Sound Vib. 2003;265:935–952.
[27] Madeira JFA, Araújo AL, Mota Soares CM, et al. Multiobjective optimization for vibration reduction in composite plate structures using constrained layer damping. Comput Struct. 2020;232:105810.
[28] Sunar M, Rao SS. Recent advances in sensing and control of flexible structures via piezoelectric materials technology. Appl Mech Rev. 1999;52:1–16.